

UCSF

UC San Francisco Electronic Theses and Dissertations

Title

Advanced Quantitative MR Imaging for Detecting Early Cartilage Degeneration

Permalink

<https://escholarship.org/uc/item/1mj961kf>

Author

Chandramohan, Dharshan

Publication Date

2013

Peer reviewed|Thesis/dissertation

Advanced Quantitative MR Imaging for Detecting Early Cartilage
Degeneration

by

Dharshan Chandramohan

THESIS

Submitted in partial satisfaction of the requirements for the degree of

MASTER OF SCIENCE

in

Biomedical Imaging

in the

GRADUATE DIVISION

of the

UNIVERSITY OF CALIFORNIA, SAN FRANCISCO

Copyright 2013

by

Dharshan Chandramohan

Acknowledgement

I would like to acknowledge my committee chair and mentor, Professor Xiaojuan Li, for her oversight and guidance, as well as the other members of my committee: Professor Sharmila Majumdar, Professor Thomas Link, and Professor Alastair Martin. I would also like to acknowledge and thank Julien Rivoire for his assistance with the experiments, and Weitian Chen for assistance with the sequences. I would like to thank Yu Zhang, Lauren Tufts, Shiree Segev, and Nicole Bronson for their help with scans.

This project was funded by a grant from GE.

I would like to dedicate this work to my parents and my sister for their unwavering support.

Advanced Quantitative MR Imaging for Detecting Early Cartilage Degeneration

Dharshan Chandramohan

Abstract

Magnetic Resonance Imaging (MRI) of cartilage offers unique insights into biochemical and microstructural processes of degeneration that might be useful in characterizing the early stages of Osteoarthritis. Quantitative MR imaging sequences enable us to map magnetic relaxation parameters of the tissue, including $T_{1\rho}$ and T_2 , which are highly sensitive to microscopic changes in cartilage. Different imaging strategies and mathematical models have been used to quantify $T_{1\rho}$. In this study we compare two strategies for $T_{1\rho}$ imaging: the SPGR-based MAPSS sequence, and the FSE-based CUBE sequence. The sequences were evaluated using simulation, phantom scans, and *in vivo* human scans. The CUBE sequence appears to outperform the MAPSS sequence in terms of SNR efficiency and repeatability on the basis of phantom and human studies. The CUBE sequence was then used to evaluate the feasibility of performing multi-exponential $T_{1\rho}$ quantification in a 63 TSL scan of a porcine knee specimen. The multi-exponential $T_{1\rho}$ procedure was able to identify two spin populations, even when the number of TSLs used to fit the model was reduced to 16. This data suggests the feasibility of performing multi-component $T_{1\rho}$ imaging *in vivo*, especially if combined with advanced accelerating techniques in the future. The results from this study need to be confirmed by larger scale studies.

TABLE OF CONTENTS

ACKNOWLEDGEMENT	iii
ABSTRACT	iv
LIST OF FIGURES	vi
LIST OF TABLES	vii
INTRODUCTION	1
MATERIALS AND METHODS	5
RESULTS AND DISCUSSION	10
CONCLUSION	21
REFERENCES	22

LIST OF FIGURES

Figure 1: $T_{1\rho}$ Phantom Schematic	p. 7
Figure 2: MAPSS Simulation	p. 10
Figure 3: 2-Component MAPSS Simulation	p. 11
Figure 4: CUBE Simulation	p. 12
Figure 5: Varied ETL CUBE Simulation	p. 12
Figure 6: Phantom Quantification Results	p. 13
Figure 7: Phantom Line Profiles	p. 15
Figure 8: Representative <i>In Vivo</i> Data	p. 17
Figure 9: Multi-exponential Fit Simulation	p. 18
Figure 10: Multi-exponential Fit Images	p. 19
Figure 11: Representative Multi-exponential Spectrum	p. 20

LIST OF TABLES

Table 1 (Sequence Parameters)	p. 6
Table 2 (SNR Efficiency)	p. 15
Table 3 (<i>in vivo</i> Repeatability)	p. 16

Introduction

Osteoarthritis (OA) is a debilitating condition which results from the degeneration of articular cartilage. It is estimated that 10-12% of the adult population in the United States suffers from symptomatic OA, a proportion which is expected to double by the year 2020 [1]. MR Imaging has become prominent as a methodology for investigating cartilage damage. Conventional MR Imaging is useful in evaluating morphological changes in articular cartilage associated with OA, and quantitative MR relaxation time mapping has been shown to be sensitive to microstructural and biochemical changes in cartilage which can help to identify earlier stages of the disease [2].

The microstructure of cartilage consists of a small number of cells, called chondrocytes, embedded in an extracellular matrix composed mainly of collagen fibers, proteoglycans (PG), and water. The cartilage is composed of three layers defined by the orientation of the collagen fibers in the matrix. The superficial zone consists of fibers oriented parallel to the articular surface, the transitional zone contains randomly oriented fibers and the deep (radial) zone contains fibers oriented perpendicular to the subchondral bone [3].

Changes in the biochemical content of the cartilage microstructure have been associated with changes in the MR relaxation properties of articular cartilage. Specifically, the transverse relaxation time (T_2) is associated with integrity of the collagen matrix and water content of the tissue. The spin-lattice relaxation time in the rotating frame ($T_{1\rho}$) has been associated with proteoglycan and other macromolecular changes in cartilage as well as water content [3].

Quantitative MR Imaging Sequences

Magnetization-prepared sequences with long readout trains conditioned to minimize signal variation, such as the MAPSS [7] or CUBE [8,9] sequences, can be used to image relaxation times *in vivo*. Both sequences consist of a magnetization preparation step followed by an imaging acquisition step.

The magnetization preparation for T_2 quantification is based on the Carr Purcell Meiboom Gill (CPMG) experiment, and consists of a 90° pulse to tip the magnetization in the transverse plane, followed by a train of 180° refocussing pulses lasting for a duration “TE”, terminating in a 90° pulse which tips the magnetization back to the longitudinal direction. The $T_{1\rho}$ magnetization preparation employs a similar strategy, replacing the train of 180° refocussing pulses with a long pulse of a particular spin-locking frequency, applied over a duration known as the time of spin-locking (TSL), which holds the magnetization along an axis in the rotating frame in order to measure spin-lattice relaxation effects in the rotating frame.

Both the MAPSS and CUBE sequences utilize the same magnetization preparation step for measuring a particular relaxation parameter; the two sequences differ, however, with respect to the image acquisition scheme employed. The MAPSS sequence uses a spoiled gradient echo (SPGR) readout train to image the conditioned longitudinal magnetization. The tip angles during the readout are modulated to compensate for T_1 relaxation so that the final contrast in the image reflects only the prepared magnetization. The 3D MAPSS sequence acquires lines of k -space in a segmented fashion, where the number of lines (or views) per segment (VPS)

determines the length of the readout train. The CUBE sequence images the conditioned magnetization using a fast spin-echo readout train. The flip angles used during the readout are less than 180° , however, and are also modulated to minimize relaxation effects. The 3D CUBE sequence also acquires lines of k -space in a segmented fashion, and the view ordering and echo train length (ETL) play a role in minimizing contrast due to relaxation effects during the readout.

These sequences are used to generate multiple images with different $T_{1\rho}$ or T_2 weighting, based on the TSL or TE of the each image, respectively. The signal in each of the varied TE or TSL images is used to fit the relaxation parameter in each voxel based on the following equations:

$$S(\vec{r}, TSL) = S_0 e^{-\frac{TSL}{T_{1\rho}(\vec{r})}}$$

or

$$S(\vec{r}, TE) = S_0 e^{-\frac{TE}{T_2(\vec{r})}}$$

where S_0 is a constant scale factor which is fit along with the relaxation parameter of interest (i.e., $T_{1\rho}$ or T_2). Some models fit an additional additive constant to account for a nonzero baseline of the decay curve.

It is an open question whether the SPGR-based MAPSS and the FSE-based CUBE sequences perform equivalently with respect to quantification accuracy, signal-to-noise (SNR) efficiency, and repeatability.

Multi-exponential signal modeling

Recent *ex vivo* experiments with animal cartilage specimens have shown that a more complete picture of the relaxation behavior in the tissue can be obtained by using multi-exponential fitting of the relaxation signal to generate a $T_{1\rho}$ or T_2 spectrum for the tissue. Wang and Xia performed multi-component $T_{1\rho}$ and T_2 quantification on bovine nasal cartilage to characterize the dependence of the multi-component nature of the $T_{1\rho}$ and T_2 relaxation on various experimental factors [4]. Their experiments demonstrate that in many cases the multi-component model improves the fit of the relaxation curve for both $T_{1\rho}$ and T_2 . For both $T_{1\rho}$ and T_2 , longer components are associated with free water whereas short T_2 components are associated with macromolecule-bounded water [5].

Reiter, et al. [6] show that multi-exponential fitting improves the specificity of cartilage biochemical characterization in enzymatically degraded cartilage specimens. Mono-exponential fitted T_2 values increased significantly after enzyme degradation of the samples, though the effect was nonspecific. Multi-exponential fitting, however, identified changes in the weights of specific T_2 components which differed between proteoglycan-specific enzymatic degradation and collagen-specific enzymatic degradation.

Both of the previously mentioned studies utilized robust but technically demanding MR spectroscopic and imaging techniques which are unlikely to prove feasible in the clinic. Our interest was in extending this work using an imaging sequence that is appropriate for clinical studies. Specimen imaging and spectroscopic studies have the luxury of using painstakingly long acquisition times and are relatively free from constraints on the amount of RF power that can be administered

to the tissue. For *in vivo* imaging, acquisition time and RF dose, as measured by the Specific Absorption Rate (SAR), are limiting factors. Consequently, the main impediment to using a multi-exponential model is the extensive amount of data required. Thus an important objective of this study was to attempt to characterize the minimum amount of data required for a clinically feasible, robust multi-component relaxation time quantification experiment using an optimized imaging sequence.

In this study we have focused on optimal methods for characterizing $T_{1\rho}$ relaxation in cartilage. First, we aimed to compare the CUBE and MAPSS sequences to determine which imaging strategy is better for quantitative $T_{1\rho}$ mapping. Then we hoped to determine the limitations that exist for multi-exponential $T_{1\rho}$ quantification using either of these imaging sequences, designed for use in humans.

Materials and Methods

Sequence Simulations

In order to compare the MAPSS and CUBE strategies the two acquisition schemes were first modeled in simulation. We designed imaging simulations for each sequence in MATLAB (MathWorks, Natick, MA, USA) to develop an intuition of how the signal evolution during the imaging segment would contribute to image quality. The MAPSS simulation modeled the Bloch Equation for the spoiled gradient-recalled signal for each echo in the readout train. Under ideal conditions the flip angle-modulated echo train should compensate for any relaxation effects. RF chopping, which is used in the sequence to eliminate the dependence of the signal on the equilibrium magnetization, was also simulated. The CUBE simulation modeled

relaxation effects on the signal for a point object represented by a small population of spins at the center of the simulated field of view. The point spread function for the simulated point objects from both the MAPSS and CUBE simulations was convolved with the physical representation of the object by multiplying the Fourier transform of the object with the signal weighting for the readout in accordance with the view ordering scheme for the imaging sequences. Using this paradigm we were able to develop an intuition regarding quantification accuracy and potential theoretical limitations to the two imaging paradigms.

Imaging Sequence Comparison

Sequence	MAPSS	CUBE
TR (ms)	1200	1247
Resolution (mm)	0.5469 x 0.5469	0.5469 x 0.5469
Acquisition Matrix	256 x 256	256 x 256
Slice Thickness (mm)	4	2
TSLs (ms)	1, 4, 8, 12, 20, 50, 80	1, 4, 8, 12, 20, 50, 80
Spin-lock frequency (Hz)	500	500
VPS/ETL	64	35

Table 1: Imaging Sequence Parameters

Imaging to compare the two acquisition strategies was performed on phantoms and human subjects. All imaging was performed on a 3-Tesla GE MR750

WideBore scanner. For both phantom and *in vivo* human studies two repetitions of each sequence using a $T_{1\rho}$ -mapping paradigm consisting of 7 TSL images per acquisition, sampling the decay curve at TSL = 1, 4, 8, 12, 20, 50, 80 ms. Additional imaging parameters can be found in Table 1. The CUBE sequence was run with an echo train length of 35, and a 2mm slice thickness, whereas the MAPSS sequence had an echo train length of 64 and a 4mm slice thickness. Because the RF chopping in the MAPSS sequence necessitates twice as many excitations as the CUBE for the same matrix size these parameters were selected to cause the two sequences to take approximately the same time to run.

The phantom scans were conducted using phantoms consisting of 7 or 8 conical vials filled with agarose gel. The agarose concentrations in the vials were 1, 2, 3, and 4% by weight/volume and vials of each concentration were bound together to generate the phantoms as shown in Figure 1.

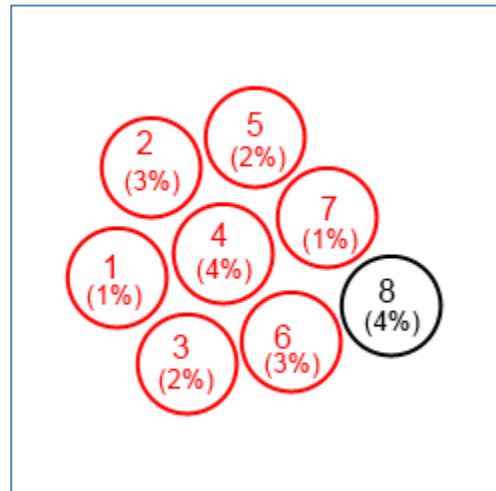


Figure 1. Schematic of the $T_{1\rho}$ imaging phantom. Two phantoms were used, consisting of 7 and 8 agarose-filled conical vials, respectively. The values in parentheses correspond to the percent agarose concentration by weight of the gel in that vial.

In addition to the $T_{1\rho}$ sequences, each sequence was acquired with two repetitions of TSL = 1ms and 80ms to estimate SNR for both

the relatively high signal first TSL, and relatively low signal final TSL with each sequence. SNR was estimated as the mean in each region of interest (ROI) of the average voxel intensity between the two repetitions, divided by the standard deviation across the ROI of the difference in voxel intensity between the two

repetitions. Maps of $T_{1\rho}$ were generated for each repetition of the CUBE and MAPSS $T_{1\rho}$ sequences using a two parameter model and statistics were computed for ROIs placed in each of the agarose vial phantoms. The percent coefficient of variation in $T_{1\rho}$ was computed between repeated scans across all ROIs. Line profiles were also plot through the phantoms to evaluate differences in blurring between the two sequences.

To compare the sequences *in vivo* we imaged the right knees of five healthy human subjects: three males and two females between 21 and 35 years of age. In addition to the two repetitions of each $T_{1\rho}$ sequence mentioned above, a high resolution T_2 -weighted CUBE (3D FSE) scan was acquired for guiding anatomical segmentation of the cartilage. Knee cartilage was segmented semi-automatically, using in-house developed software, into 6 compartments (see Figure 8): the Lateral Femoral Condyle (LFC), Medial Femoral Condyle (MFC), Lateral and Medial Tibial Cartilage (LT, MT), Patellar Cartilage (PAT), and Trochlear Cartilage (TRO). These segmentations were then transferred to the $T_{1\rho}$ maps generated from the $T_{1\rho}$ sequences by registering the structural CUBE image to the high-signal first TSL image of each $T_{1\rho}$ sequence. In cases where the registration was poor the ROIs were manually edited using the first TSL image. As with the phantom, $T_{1\rho}$ maps were generated for each sequence run using a two parameter fit and statistics were calculated for each ROI. Repeatability was determined by the percent coefficient of variation between repetitions of the sequence across all subjects.

Specimen Scan for Multi-exponential Analysis

To evaluate whether one could feasibly and faithfully reconstruct a multi-component $T_{1\rho}$ spectrum given a relatively constrained acquisition on a clinical scanner, as opposed to the extensive acquisition schemes used in the literature, we first validated our protocol in simulation. As done previously in the literature, we simulated the signal at each TSL as the weighted sum of contributions from each $T_{1\rho}$ component.

$$y(TSL) = y_0 \sum_{m=1}^M w_m e^{-\frac{TSL}{T_{1\rho,m}}} + \eta(0, \sigma)$$

Where y_0 is an arbitrary scale factor for the signal, M is the number of simulated $T_{1\rho}$ components, w_m and $T_{1\rho,m}$ are the fraction and $T_{1\rho}$ value, respectively, of each $T_{1\rho}$ component, and $\eta(0, \sigma)$ is additive, Gaussian-distributed noise. The quantity y_0/σ represents the signal to noise ratio of the simulated signal. For our simulation we used an SNR value consistent with the measured SNR for the low-signal, final TSL image in our phantom study. Our simulated signal was then fit using the non-negative least squares (NNLS) method in MATLAB.

Imaging was performed using a porcine knee specimen, which had been acquired five days prior to the scan and kept refrigerated without any special preservation until the time of the scan. Images were acquired using the CUBE $T_{1\rho}$ sequence with 63 TSLs. The first TSL was 1ms, followed by TSLs of 2 to 124ms spaced by 2ms. The full set of images was acquired in 9 repetitions of the imaging sequence, with 7 TSLs per acquisition. The TSLs used in each acquisition were interleaved so as not to overload any one acquisition, with an eye towards SAR constraints. The 63 TSL data was fit using the two parameter mono-exponential model used in the phantom

and *in vivo* studies as well as using the NNLS method for multi-exponential quantification.

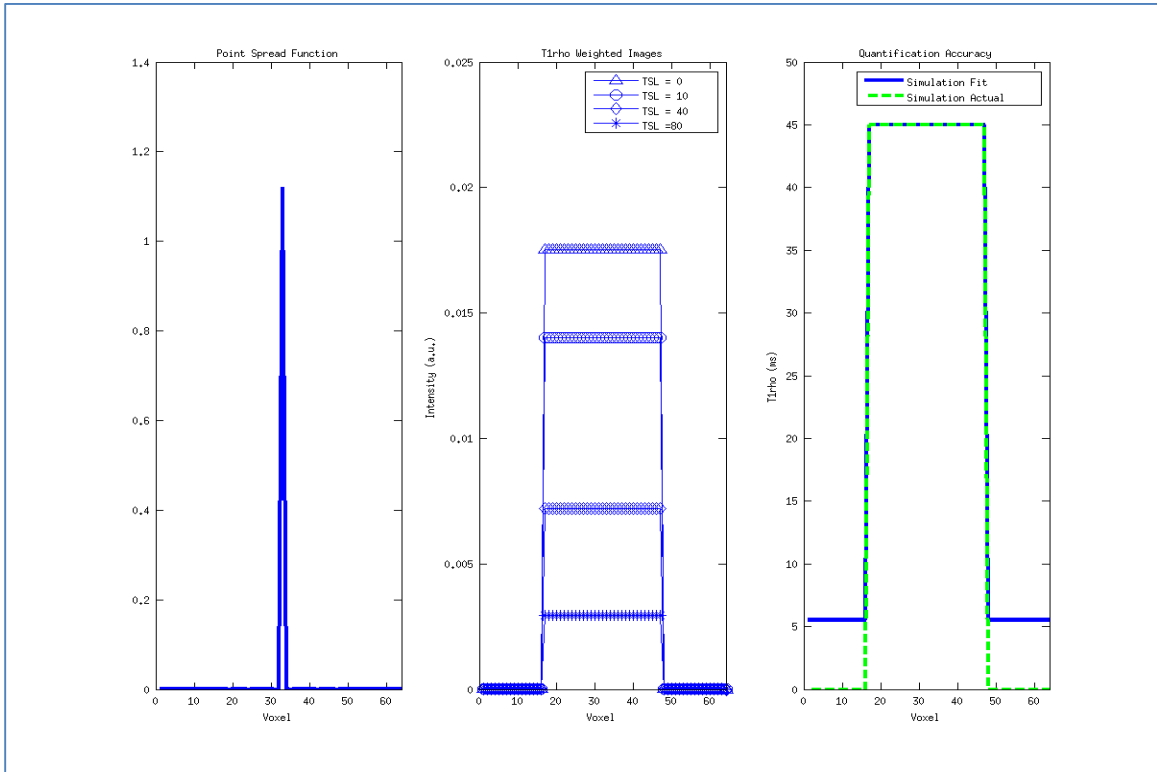


Figure 2. MAPSS Simulation Result: Point spread function (left), T1rho-weighted TSL Images (center), and Reconstructed T1rho Map (right).

Results and Discussion

Simulation Results

The MAPSS simulation represents an idealized MAPSS acquisition with no noise. Figure 2 illustrates the effect of flip angle modulation and RF chopping in compensating for relaxation effects. In this ideal case for the spoiled gradient-recalled

acquisition only T_1 effects need to be compensated for by flip angle modulation, while

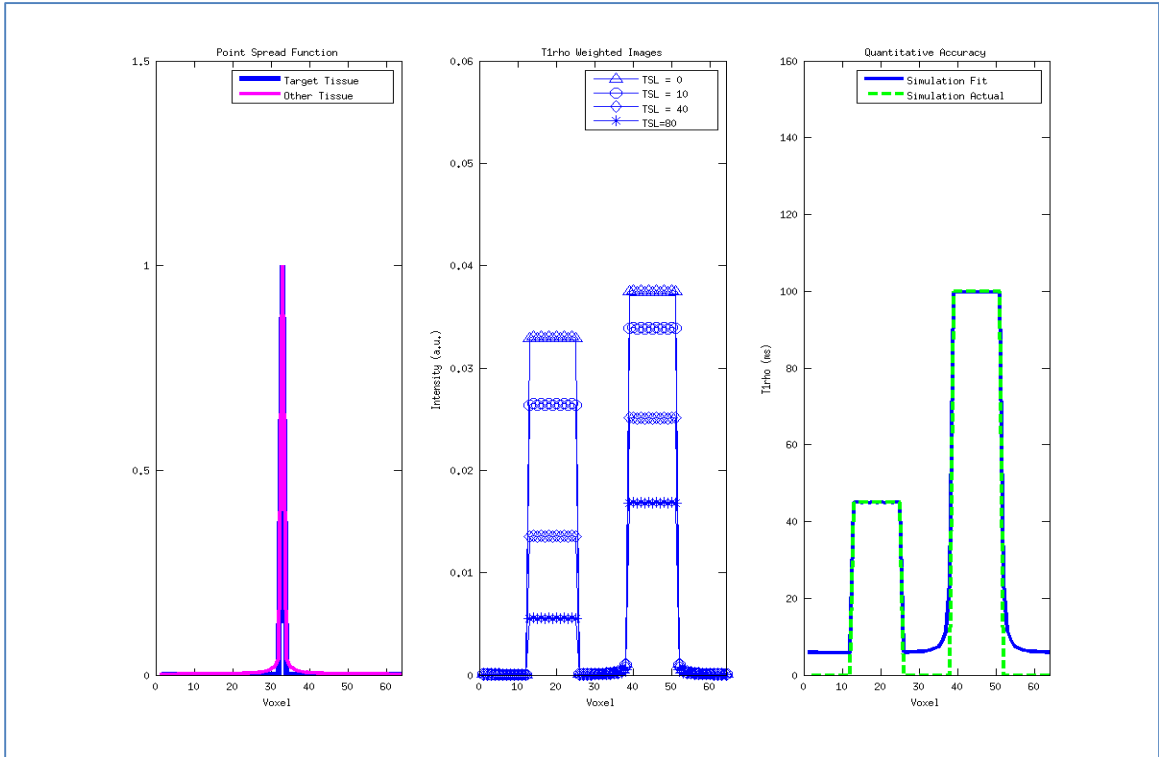


Figure 3. Demonstration of blurring due to T_1 effects. The non-target tissue (on the right in $T_1\rho$ weighted images and $T_1\rho$ map) has T_1 roughly twice that of the target tissue. Thus flip angle-modulation does not fully correct relaxation effects resulting in blurring.

RF chopping prevents baseline DC signal offsets between the different TSL images. As a result the point spread function remains tight and the TSL images reflect $T_{1\rho}$ weighting in such a way as to ensure accurate quantification. Since the flip train is optimized using an assumed T_1 value for a given target tissue, tissues in the imaged object which have dramatically different T_1 properties will have a different point

spread function, producing potential artefacts in the resulting images (Figure 3).

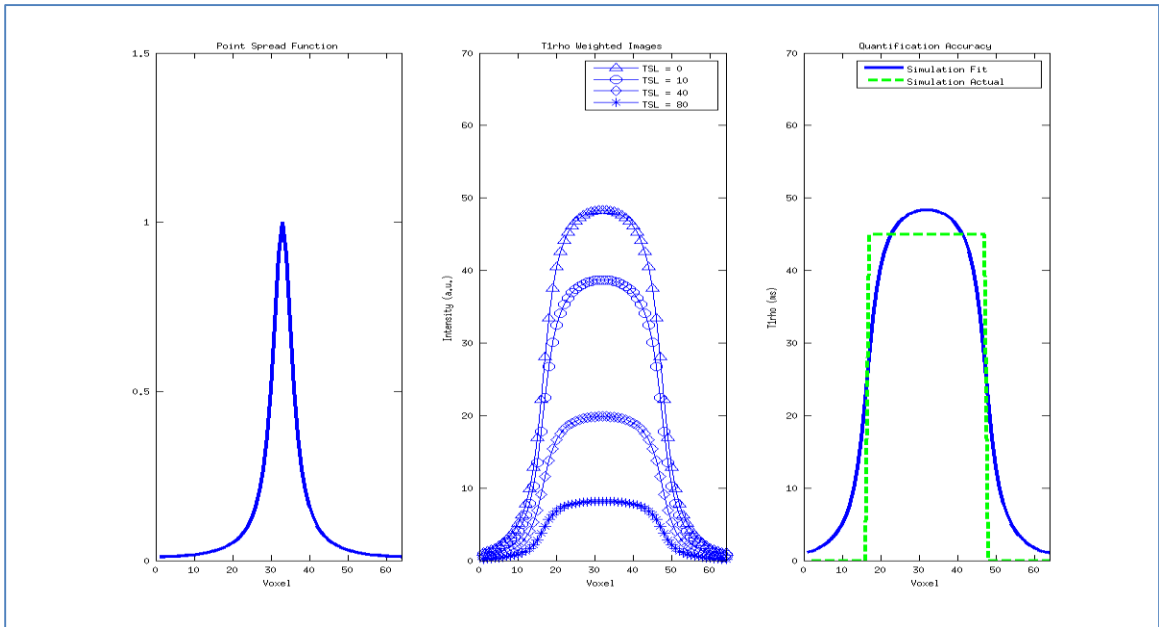


Figure 4. CUBE Simulation Results: (left) Point Spread Function, (center) T1rho Weighted Images, (right) Simulated Quantification Result.

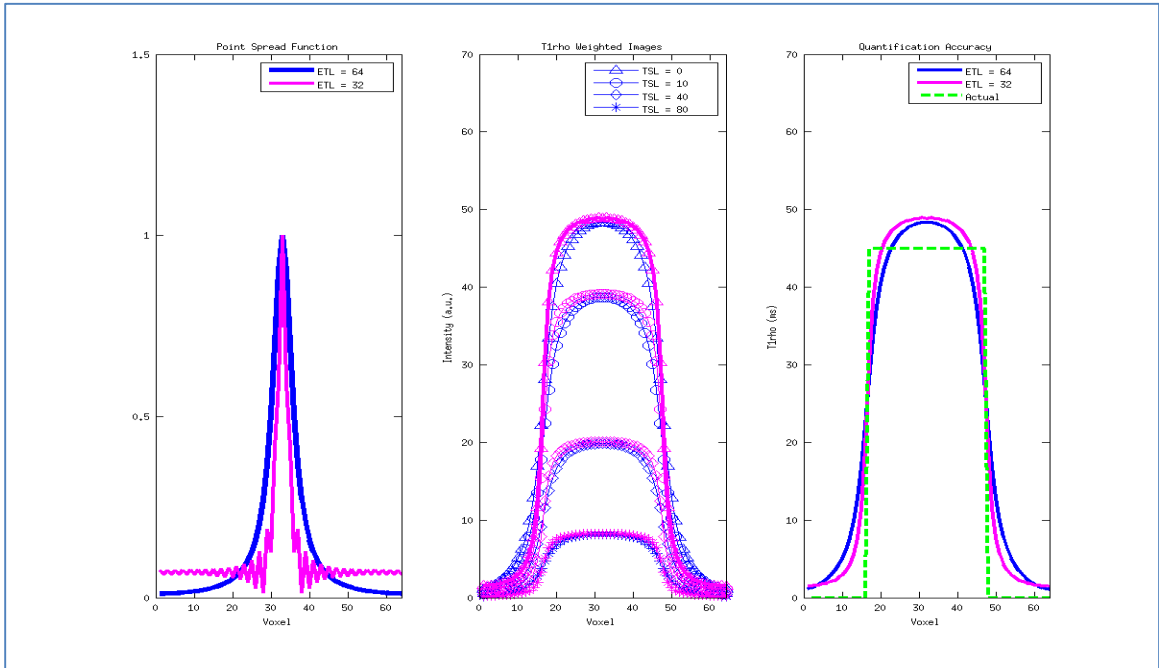


Figure 5. Shortening the ETL produces a narrower Point Spread Function, which results in less blurring of the T1rho Weighted Images and T1rho Map.

The CUBE sequence, on the other hand, is susceptible to T2 decay during the echo train, and though flip angle-modulation is used to compensate for this to a

certain extent, the remaining signal decay effectively filters k -space. The resulting point spread function is not as narrow as the MAPSS and there is visible blurring in both the TSL images and the computed $T_{1\rho}$ map, as seen in Figure 4. This effect can be mitigated by reducing the echo train length, as shown in Figure 5.

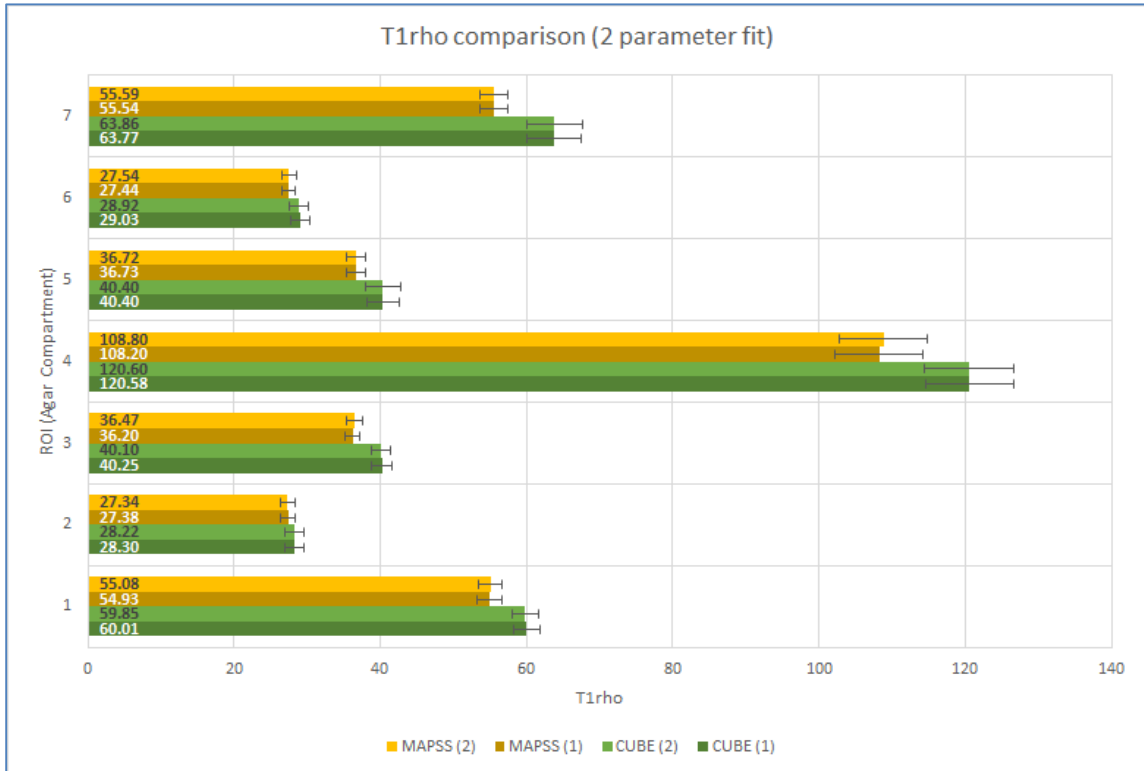


Figure 6. Mean $T_{1\rho}$ values for ROIs for 7 homogeneous agarose phantoms. Error bars represent standard deviation of $T_{1\rho}$ value in the ROI.

Phantom Imaging Results

Results of the repeatability experiment with the 7-vial phantom are plotted in Figure 6. From this data we can gather that the CUBE and MAPSS sequences both appear to produce comparable results for $T_{1\rho}$ quantification. There also appears to be a trend whereby the quantified $T_{1\rho}$ from the CUBE sequence exceeds the quantified

$T_{1\rho}$ from the MAPSS sequence in compartments for which the $T_{1\rho}$ value is long. In terms of quantitative repeatability, the percent coefficient of variation between repeated scans is 0.14% for the CUBE sequence and 0.37% for the MAPSS sequence.

In terms of signal-to-noise ratio for both the high-signal, 1ms TSL image and the low-signal, 80ms TSL image the CUBE sequence outperformed the MAPSS sequence. Raw SNR values averaged over the 8 ROIs are 87.66 for the CUBE compared to 65.48 for the MAPSS for the 1ms TSL image, and 24.62 for the CUBE versus 15.60 for the MAPSS for the 80ms TSL image. When normalized by voxel size and acquisition time the SNR efficiency at 1ms TSL of 11.51 for the CUBE and 4.22 for the MAPSS; at 80ms TSL the SNR efficiency is 3.14 for the CUBE and 1.05 for the MAPSS. These results are summarized in Table 2. Ultimately the CUBE sequence demonstrates an approximately threefold increase in SNR efficiency compared to the MAPSS sequence over both TSL conditions. The effects of spoiling, inhomogeneity, and the low signal target used for flip angle optimization to satisfy the SPGR condition for the MAPSS sequence, might explain these results, since, based on these considerations, the available signal, and therefore signal-to-noise ratio should be lower for images acquired with the MAPSS sequence than those acquired with the CUBE sequence.

To investigate the potential presence of blurring in the CUBE images we plotted line profiles through the phantom images and overlaid them with line profiles through the same location in the MAPSS images. As seen in Figure 7 the CUBE sequence does appear to show slight blurring in the phase encode direction. The

<i>Table 2</i>	TSL = 1 ms		TSL = 80 ms	
Sequence	Raw SNR	SNR Efficiency	Raw SNR	SNR Efficiency
MAPSS	65.48	4.22	15.60	1.05
CUBE	87.66	11.51	24.62	3.14

width of the phantom at half maximum appears to be greater by one to two voxels (0.5469 to 1.0938 mm). This is as we expected from our simulation data. It is difficult to assess via comparison whether this blurring is present in the quantitative map for the CUBE sequence due to the fact that the MAPSS quantitative map displays a prominent edge effect, likely due to Gibbs ringing. An optimally short echo train (ETL = 35) and the use of parallel imaging to accelerate by a factor of 2 in the phase encode direction most likely contributed to minimizing blurring effects resulting from relaxation during the echo train.

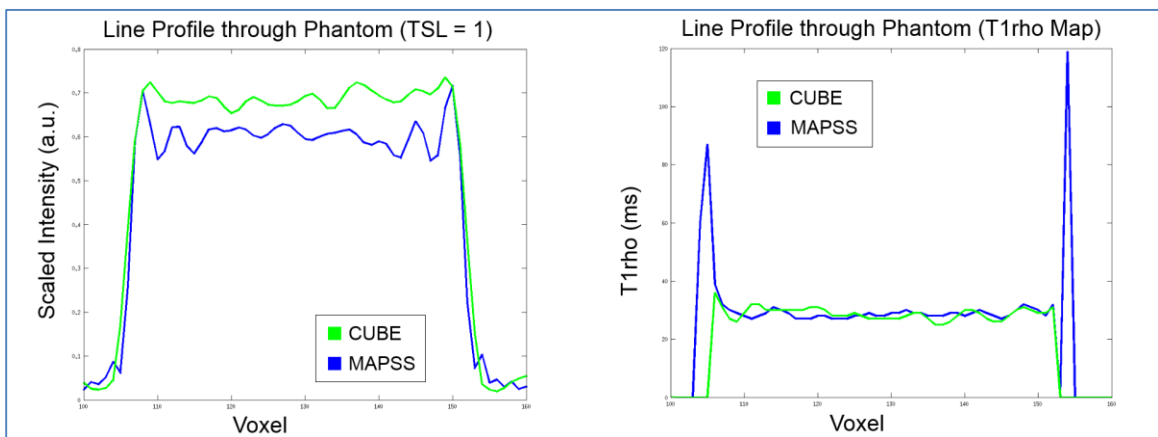


Figure 7. Line profiles show expected blurring in CUBE relative to MAPSS.

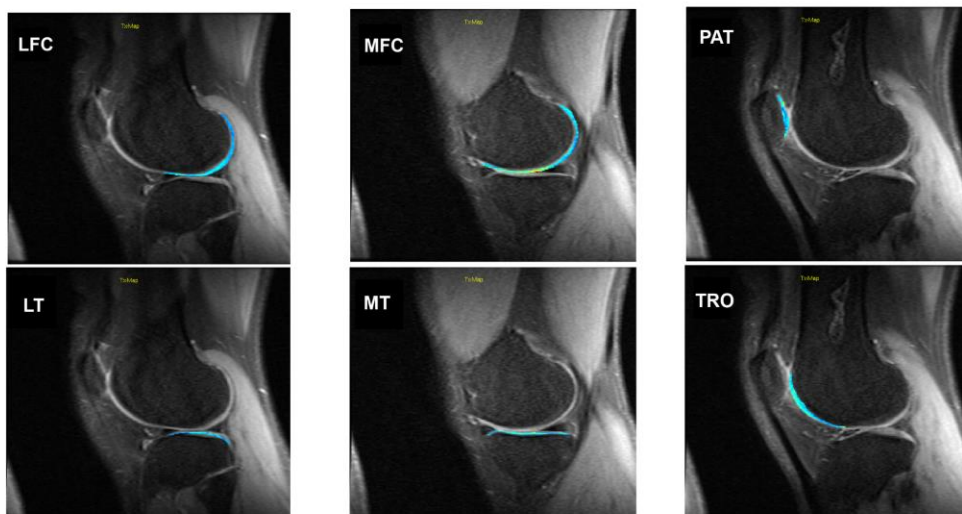
Human Subject Repeatability

Table 3: In Vivo Human Scans – Repeatability Data

ROI	MAPSS %CV	CUBE %CV
LFC	9.23	1.78
LT	5.17	5.10
MFC	6.87	2.62
MT	6.89	5.81
PAT	5.88	2.18
TRO	6.40	2.14

Figure 8 shows quantitative $T_{1\rho}$ map data in each ROI for a representative subject overlaid on the first TSL image. Repeatability data from the human subject scans is summarized in Table 3. Repeatability appears to be significantly better for the CUBE sequence than for the MAPSS sequence. These data, however, are to be taken with the caveat that it is possible that registration error between the structural images used for segmentation and the MAPSS $T_{1\rho}$ sequence images may be confounding these values. The percent coefficient of variation recorded in this study for the LFC, for example, is in excess of the coefficient of variation for $T_{1\rho}$ quantified by the MAPSS sequence as reported in the literature [11].

CUBE



MAPSS

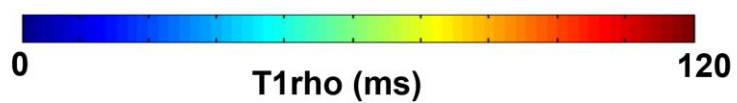
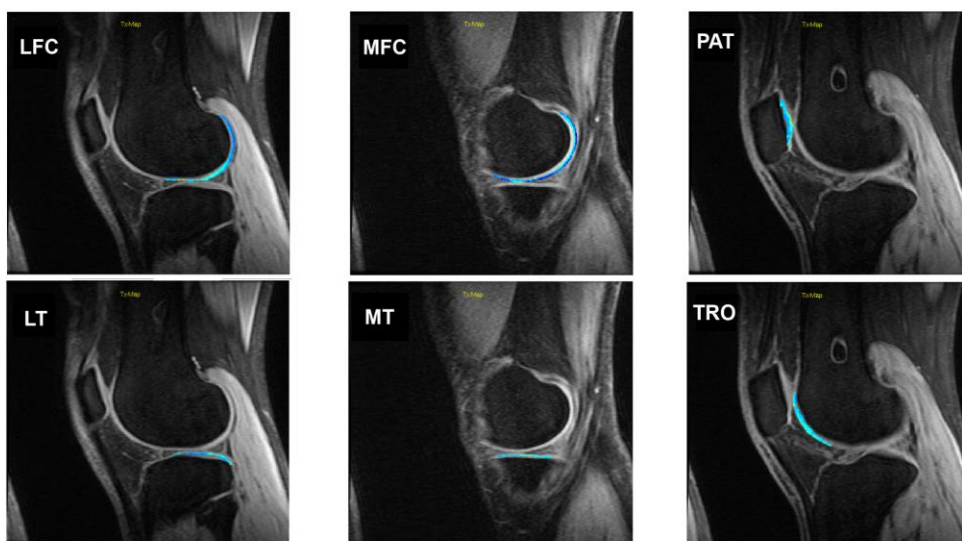


Figure 8. Quantitative data in each ROI from a representative subject superimposed on first TSL image.

Multi-exponential Specimen Quantification

The results for simulating a multi-exponential $T_{1\rho}$ quantification experiment using an acquisition scheme similar to our specimen scan are shown in Figure 7. This simulation was performed with an SNR roughly half the SNR measured in the phantom study for a TSL of 80, which we expect to be comparable to high TSL *in vivo* images. This proof of concept indicates that we should be able to reconstruct the underlying $T_{1\rho}$ distribution using our limited imaging acquisition with comparable efficacy as the prohibitively long acquisition schemes used in the literature for quantifying multi-exponential $T_{1\rho}$ relaxation in *ex vivo* specimens.

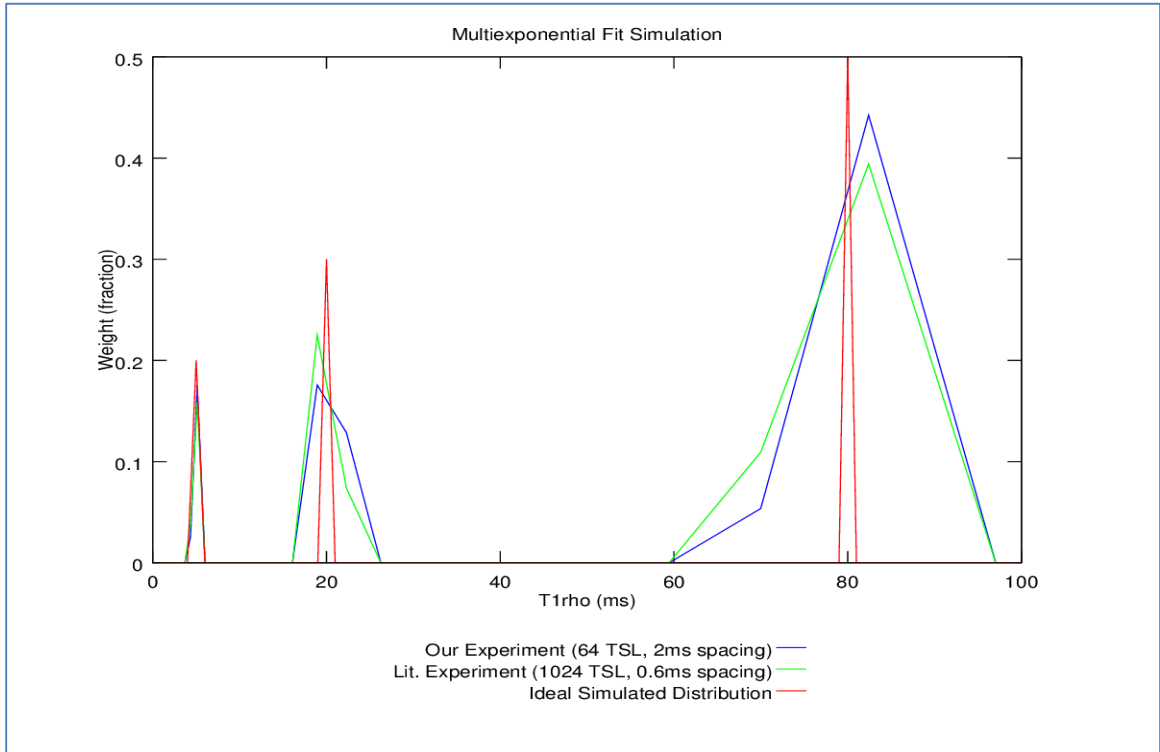


Figure 9. Proof of concept: our planned specimen imaging experiment should perform comparably with literature experiments for identifying multiple $T_{1\rho}$ populations.

MAPSS of $T_{1\rho}$ and weights for the respective $T_{1\rho}$ populations as produced from multi-exponential NNLS fitting of the 63 TSL CUBE scan of the porcine knee specimen are shown in Figure 10. Most voxel $T_{1\rho}$ spectra contained two peaks, with a handful of voxels containing four peaks. The third and fourth peaks in these voxels however did not have a weights which exceeded 3%, which has been used in the literature as a cut-off value for detecting actual peaks. The short $T_{1\rho}$ peak for the voxels in the LFC, as identified in Figure 9, tends to be extremely short: typically less than 10ms. This peak according to the weight image tends to make up between 0 and 20% of the spins in the voxel. The second compartment identified by the NNLS fitting appears to mirror the mono-exponential result, with $T_{1\rho}$ values ranging from approximately 70 to 160.

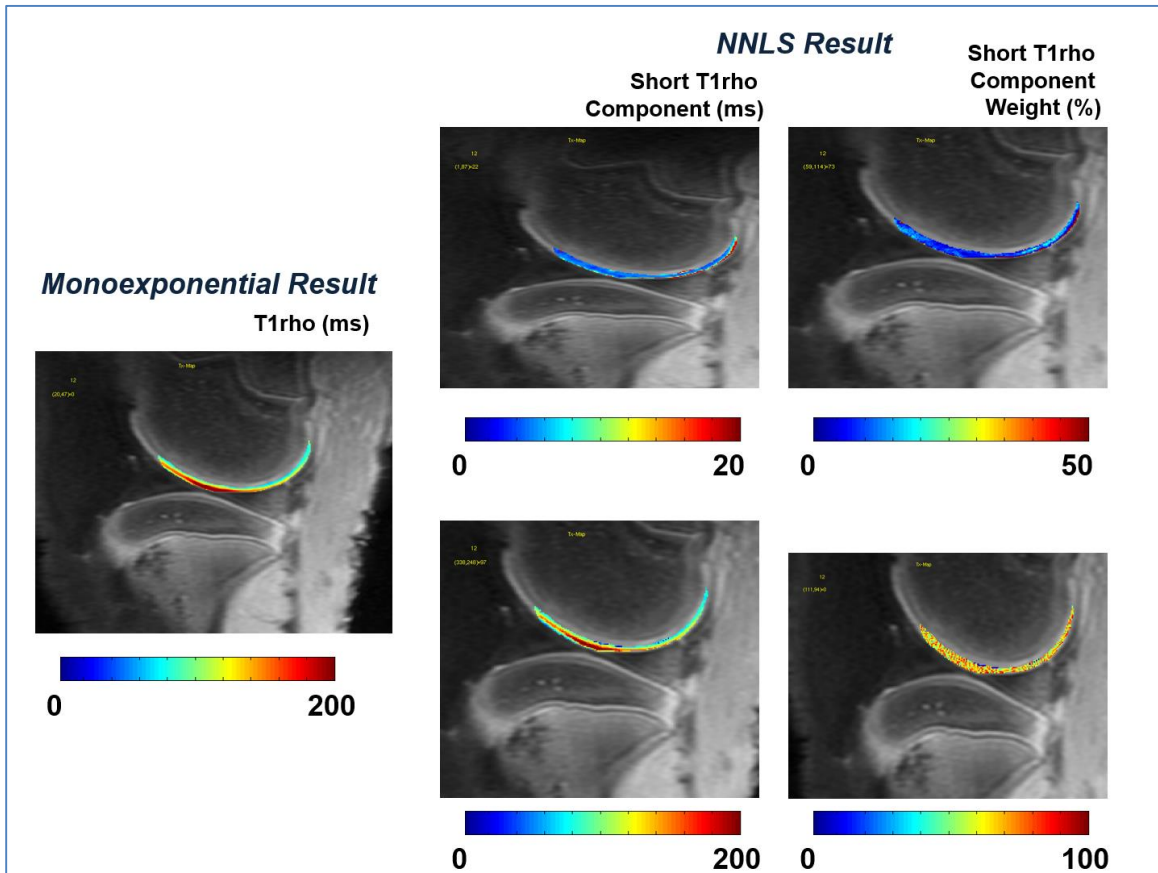
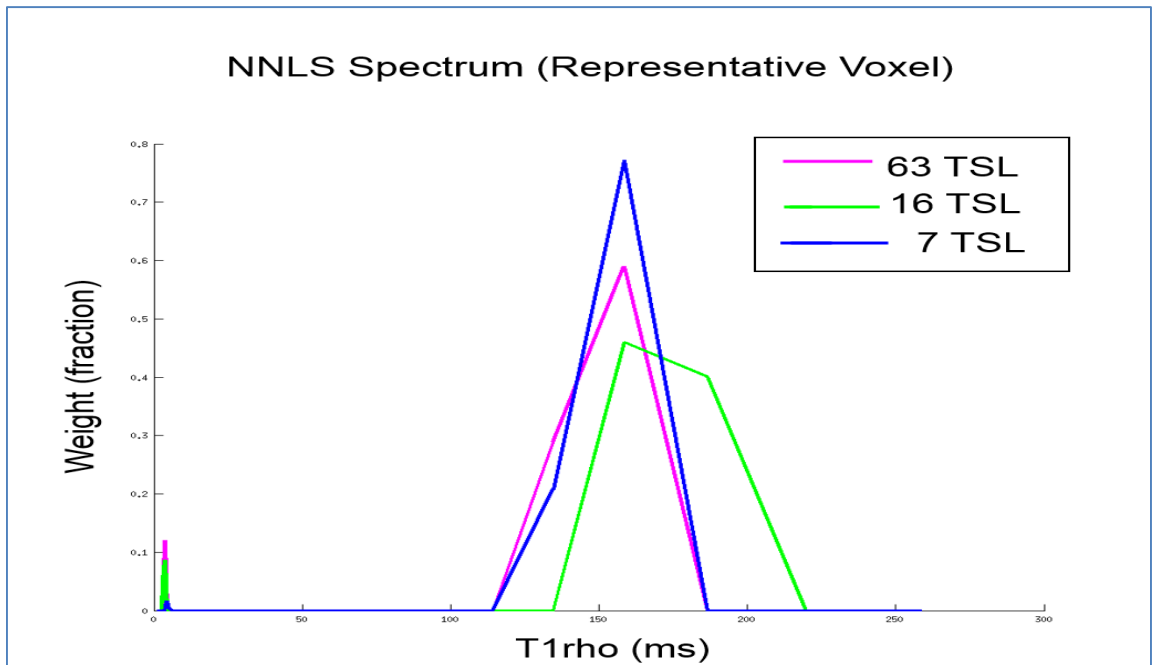


Figure 10. Comparison of multi-component imaging result with mono-exponential fit result using all 63 TSL images.

As these $T_{1\rho}$ populations are weighted at between 70 and 100% it is sensible that the mono-exponential result is heavily skewed to represent this population of spins. These $T_{1\rho}$ values are slightly higher than expected for porcine cartilage. It is possible that the handling of the specimen may have resulted in elevated $T_{1\rho}$, specifically the delay between specimen acquisition and the time of the scan. We investigated the possibility that the fit may be affected by low signal-to-noise in the very long TSL images. However, when only the data with $TSL < 80$ were fit using a mono-exponential, two-parameter model we obtained similar values for $T_{1\rho}$.

Figure 11 shows the results of performing the NNLS fitting procedure on the signal from a representative voxel in the LFC of our porcine knee specimen using subsets of the TSL images acquired. With as few as 16 TSLs it is possible to still identify the two $T_{1\rho}$ populations present when fitting the signal using all 63 TSLs.

Figure 11. Non-negative Least Squares Multi-exponential fit of data for a representative voxel in the LFC from the porcine knee specimen scan. This data suggests that it is possible to resolve multiple $T_{1\rho}$ populations with as few as 16 TSLs.



When we use 7 TSLs, in an acquisition scheme comparable to the one used in this study for the phantom and *in vivo* human acquisitions the short-relaxing $T_{1\rho}$ component weight sinks to below the 3% threshold, suggesting that more data is required to resolve that peak.

Conclusions

Based on the studies we performed there is evidence that the fast spin-echo-based CUBE sequence has several advantages for $T_{1\rho}$ quantification over the spoiled gradient-echo-based MAPSS sequence. The CUBE sequence demonstrates better signal-to-noise efficiency – enabling the acquisition of higher resolution images in roughly the same amount of time as the MAPSS sequence and with comparable quantitative results. Our measured repeatability of the $T_{1\rho}$ quantification for the CUBE sequence also exceeds the repeatability measured for the MAPSS sequence, though these results are subject to some experimental limitations. The blurring artefact in the CUBE images is relatively minor and appears to have been partially compensated by optimizing the echo train length and employing parallel imaging. Furthermore, we have demonstrated that the CUBE sequence can be used to generate multi-exponential $T_{1\rho}$ data which could help characterize pathophysiological changes in cartilage with higher specificity than is possible with existing methods. The main limitation of this study is the small amount of data which was collected. More extensive work will be needed to validate these findings in a larger sample.

References:


1. Hunter DJ. Osteoarthritis. *Best Practices & Research Clinical Rheumatology*. 2011;25(6):801-14.
2. Roemer FW, Crema MD, Trattnig S, Guermazi A. Advances in Imaging of Osteoarthritis and Cartilage. *Radiology*. 2011. 260:332-54.
3. Li X, Cheng J, Lin K, Saadat E, Bolbos RI, Jobke B, Ries MD, Horvai A, Link TM, Majumdar S. Quantitative MRI using T1 ρ and T2 in human osteoarthritic cartilage specimens: correlation with biochemical measurements and histology. *Magnetic Resonance Imaging*. 2011;29(3):324-34.
4. Wang N, Xia Y. Dependencies of multi-component T2 and T1rho relaxation on the anisotropy of collagen fibrils in bovine nasal cartilage. *Journal of magnetic Resonance*. 2011;212:124-32.
5. Reiter D, Roque R, Lin P, Irrechukwu O, Doty S, Longo D, Pleshko N, Spencer R. Mapping Proteoglycan bound water in cartilage: improved specificity of matrix assessment using multiexponential transverse relaxation analysis. *Magnetic Resonance in Medicine*. 2011;65:377-84.
6. Reiter DA, Roque RA, Lin P-C, Doty SB, Pleshko N, Spencer RG. Improved specificity of cartilage matrix evaluation using multiexponential transverse relaxation analysis applied to pathomimetically degraded cartilage. *NMR Biomed*. 2011.
7. Li X, Han ET, Busse RF, Majumdar S. In vivo T1 ρ Mapping in Cartilage Using 3D Magnetization-Prepared Angle-Modulated Partitioned k-space Spoiled Gradient Echo Snapshots (3D MAPSS). *Magnetic Resonance in Medicine*. 2008;59:298-307.
8. Busse RF, Brau ACS, Vu A, Michelich CR, Bayram E, Kijowski R, Reeder SB, Rowley HA. Effects of Refocusing Flip Angle Modulation and View Ordering in 3D Fast Spin Echo. *Magnetic Resonance in Medicine*. 2008;60:640-49.
9. Chen W, Takahashi A, Han E. 3D Quantitative Imaging of T1rho and T2 (Abstract). *Proc Intl Soc Mag Reson Med*. 2011;19:#231.
10. Zheng XK, Xia Y. On the measurement of multi-component T2 relaxation in cartilage by MR spectroscopy and imaging. *Magnetic Resonance Imaging*. 2010; 28(4):537-45.
11. Li X, Wyatt C, Rivoire J, Han E, Chen W, Schooler J, Liang F, Shet K, Souza R, Majumdar S. Simultaneous acquisition of T1 ρ and T2 quantification in knee cartilage: Repeatability and diurnal variation. *J Magn Reson Imaging*. 2013.

Publishing Agreement

It is the policy of the University to encourage the distribution of all theses, dissertations, and manuscripts copies of all UCSF theses, dissertations, and manuscripts will be routed to the library via the Graduate Division. The library will make all theses, dissertations, and manuscripts accessible to the public and will preserve these to the best of their ability, in perpetuity.

Please sign the following statement:

I hereby grant permission to the Graduate Division of the University of California, San Francisco to release copies of my thesis, dissertation, or manuscript to the Campus Library to provide access and preservation, in whole or in part, in perpetuity.



Author Signature

17 SEPT. 2013

Date